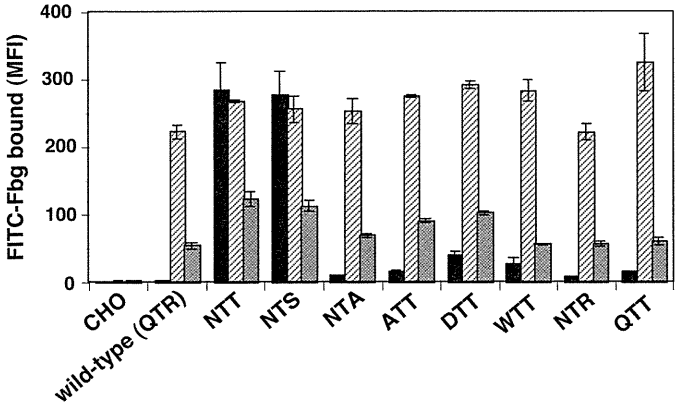


FIGURE 4. **Constitutive activation depends on the binding of *N*-glycan in the Q595N/R597T mutant.** Three amino acid residues starting from Gln-595 in the αIIb chain were mutated to various sequences. Fbg binding to the cells in the presence of 1 mM $Ca^{2+}$/1 mM $Mg^{2+}$ with a control antibody (*solid column*) or with PT25-2 (*hatched column*) and in the presence of 1 mM $Mn^{2+}$ with a control antibody (*gray column*) was examined. *MFI*, mean fluorescent intensity. *Error bars* indicate S.E.

comparable with that induced by NTT (Fig. 4). These results suggest that the introduction of virtually any sequence other than the N*X*(T/S) sequence fails to induce constitutive activation. Thus, these results indicate that the activating effect of these mutations actually depends on the attachment of a bulky *N*-glycan to these sites.

To confirm whether *N*-glycans are actually attached to the intended sites in these mutants, we next compared their molecular sizes using SDS-PAGE. If an extra *N*-glycan is indeed attached to these mutants, their molecular size should be larger than that of the wild-type. When surface-expressed αIIbβ3 was labeled with biotin and immunoprecipitated with anti-αIIb mAb, the β3 chain was always co-precipitated from the cells expressing wild-type or mutant αIIbβ3. However, the size of the mutant αIIb chain that carries an extra *N*-glycan-binding site (T478N, D589N/H591T, Q595N/R597T) was not remarkably different from that of the wild-type (supplemental Fig. S3*A*). As the size of the *N*-glycan was relatively small when compared with the entire αIIb chain, it was difficult to discriminate such small differences in molecular weight using SDS-PAGE. To circumvent this problem, the αIIb leg region encompassing amino acid residues 450–1008 was generated using a FLAG tag sequence on its N terminus. This fragment was surface-expressed and migrated as an 89-kDa band on SDS-PAGE when immunoprecipitated with PL98DF6. In contrast, a similar fragment carrying an extra *N*-glycan binding site migrated as a 91-kDa band, which is slightly larger than that of the wild type. The fragment that was not supposed to attach *N*-glycan (R597T) migrated as fast as the wild type (supplemental Fig. S3*B*). Similar results were obtained when anti-FLAG M2 was used instead of PL98DF6 (data not shown). This difference in apparent molecular weight was completely lost when the fragments were digested with peptide *N*-glycosidase F as all the fragments migrated as 69-kDa bands (supplemental Fig. S3*C*). These results clearly indicate that the mutant αIIb that carries an extra N*X*(T/S) motif indeed binds *N*-glycan to these sites.

*αIIbβ3 Activation Induced by Integrin Extension Depends on the Swing-out of the Hybrid Domain*—Takagi *et al.* (10) and Luo *et al.* (23) have reported that the outward swing of the hybrid

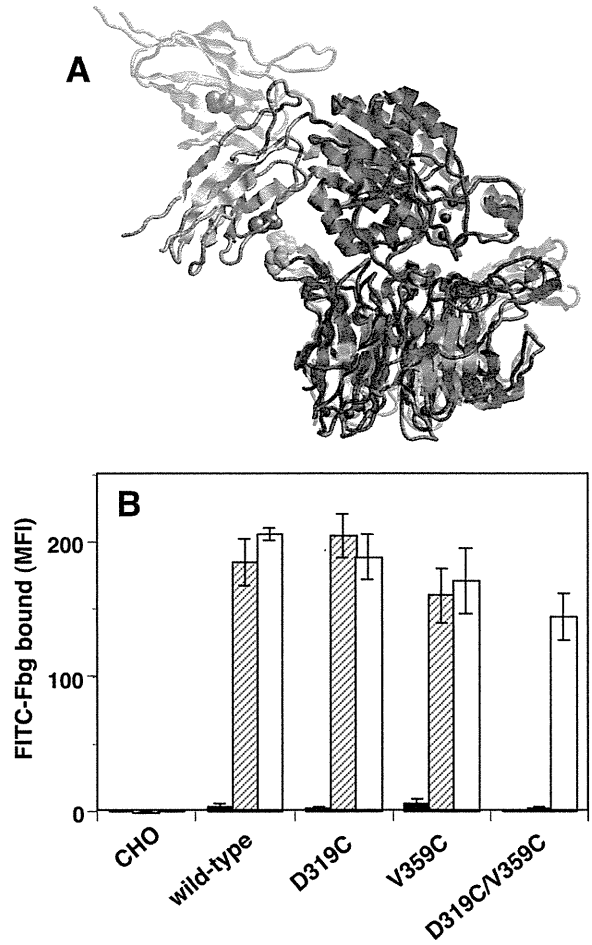


FIGURE 5. **Swing-out of the hybrid domain is required for integrin activation.** *A*, crystal structure of the αVβ3 head domains derived from the bent conformation complexed with RGD peptide is overlaid on the crystal structure of the αIIbβ3 head domains complexed with the ligand, which is shown as a *semitransparent ribbon*. In both parts of this graphic, the β-propeller domain in the α-chain is shown as a *blue ribbon*. The βA and the hybrid domains in the β3 chain are shown as *red* and *orange ribbons*, respectively. Note that Asp-319 in αIIb (Asp-306 in αV), shown as *cyan spacefill*, and Val-359 in β3, shown as *magenta spacefill*, are close to each other in the closed head (as in αVβ3) but are separated in the open head (as in αIIbβ3). *B*, to investigate the role of the swing movement of the hybrid domain in integrin activation, Asp-319 in αIIb and/or Val-359 in β3 were mutated to Cys to facilitate disulfide bridge formation between the two residues. Fbg binding to cells in the presence of 1 mM $Ca^{2+}$/1 mM $Mg^{2+}$ is shown. The *solid column* represents binding in the presence of control antibody, and the *hatched column* represents binding in the presence of PT25-2. The *open column* represents binding to cells pretreated with DTT. *MFI*, mean fluorescent intensity. *Error bars* indicate S.E.

domain is the most critical step in integrin activation. To examine whether this step is truly required for activation, the swing-out of the hybrid domain was prevented by covalently ligating the β-propeller and the hybrid domains with a disulfide bridge. The amino acid residues Asp-319 of the αIIb β-propeller and Val-359 of the β3 hybrid domain are physically close in the closed head (swing-in) conformation, whereas they are separated in the open head (swing-out) conformation (Fig. 5*A*). If these residues are simultaneously mutated to Cys, a disulfide bridge will be formed between these domains, thereby fixing the angle between the βA and hybrid regions in the closed head conformation. The 2-3 loop in blade 5 of the αIIb propeller, where Asp-319 is located, was previously shown not to partic-

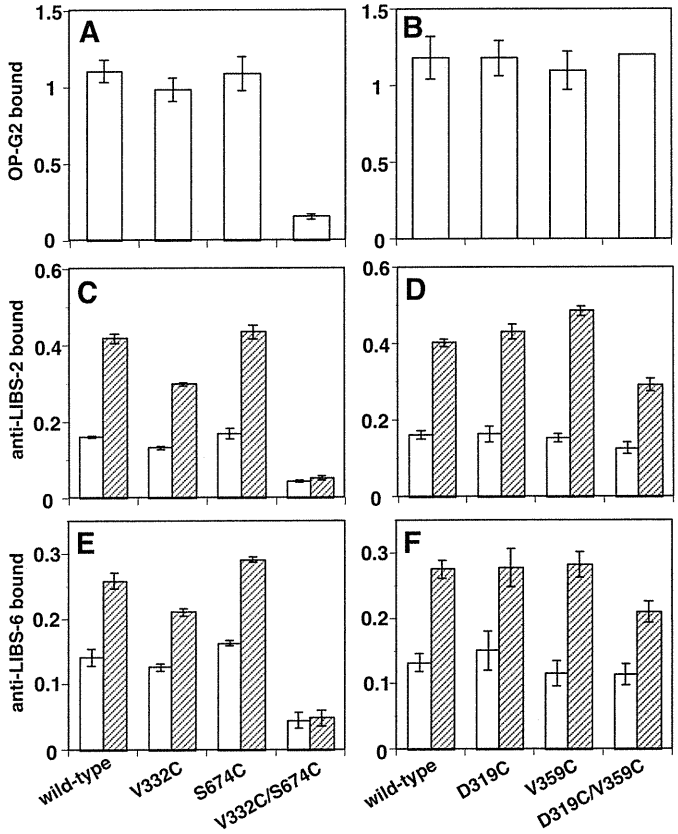


FIGURE 6. **mAb binding to cells expressing αIIbβ3 constrained in the bent conformation or in the closed head.** The binding of the ligand-mimetic mAb OP-G2 (*A* and *B*), anti-LIBS mAbs anti-LIBS2 (*C* and *D*), and anti-LIBS6 (*E* and *F*) to cells expressing αIIbβ3 constrained in the bent conformation (*A*, *C*, and *E*) or in the closed head (*B*, *D*, and *F*) was examined. Values in the *y* axis represent normalized mAb binding. The *open column* represents mAb binding in the presence of 1 mM $Ca^{2+}$/1 mM $Mg^{2+}$. The *hatched column* represents binding in the presence of 1 mM GRGDS peptide under the same cation conditions. *Error bars* indicate S.E.

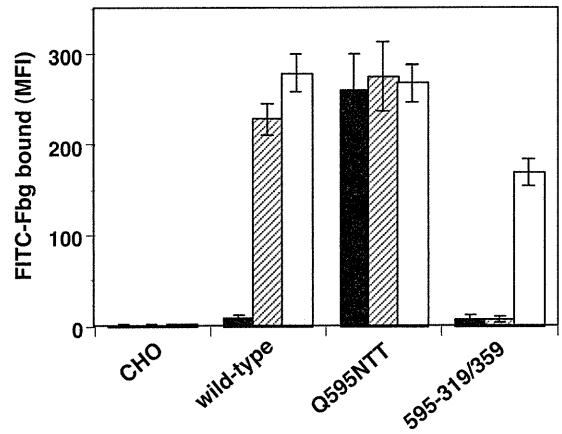


FIGURE 7. **Swing-out of the hybrid domain is required for activation induced by integrin extension.** The effect of the swing-out of the hybrid domain on extension-induced integrin activation was examined. To constrain αIIbβ3 in the extended conformation with a closed head, the Q595N/R597T and D319C/V359C mutations were combined (595-319/359). Fbg binding to the cells in the presence of 1 mM $Ca^{2+}$/1 mM $Mg^{2+}$ and the control antibody (*solid column*) or PT25-2 (*hatched column*) and Fbg binding to cells pretreated with DTT (*open column*) is shown. *MFI*, mean fluorescent intensity. *Error bars* indicate S.E.

ipate in ligand binding (24). As shown in Fig. 5*B*, single D319C or V359C mutation did not significantly affect Fbg binding. However, D319C/V359C double mutation completely abolished the Fbg binding induced by PT25-2 unless the cells were pretreated with DTT. The binding of PT25-2 was unaffected by disulfide formation (supplemental Fig. S1). Next, we examined the binding of an activation-independent ligand-mimetic mAb, OP-G2. OP-G2 has an RGD-related RYD sequence in the CDR3 and binds αIIbβ3 in almost the same fashion as Fbg, although it does not require integrin activation for binding (25). Unlike the V332C/S674C mutation, which keeps integrin in a bent conformation, the D319C/V359C mutation did not affect OP-G2 binding (Fig. 6, *A* and *B*). To examine the effect on the conformational change induced by ligand binding, the binding of anti-LIBS mAb was examined. The binding of anti-LIBS2 and anti-LIBS6 increased significantly in the presence of RGD peptide in cells expressing wild-type αIIbβ3 as well as in cells expressing the single Cys mutation V332C or S674C. However, cells expressing V332C/S674C bound significantly less anti-LIBS mAb than cells expressing wild-type αIIbβ3, and these cells did not respond to RGD peptide (Fig. 6, *C* and *E*). In contrast, cells expressing D319C/V359C showed a basal binding comparable with that of the wild type or single Cys mutants, although the response to RGD peptide was slightly attenuated (Fig. 6, *D* and *F*). These results indicate that the swing-out of the hybrid domain is only required for high affinity ligand binding and that the prevention of the swing-out does not completely inhibit the conformational change associated with ligand binding. To examine whether the swing-out of the hybrid domain is required for the activation induced by integrin extension, we combined Q595N/R597T with D319C/V359C and examined its effect on Fbg binding. The resulting 595-319/359 mutant was expected to adopt an extended with a closed head conformation. The activating effect of the Q595N/R597T mutation was completely suppressed by the D319C/V359C mutation. PT25-2 was ineffective, unless the cells were pretreated with DTT (Fig. 7). These results suggest that integrin extension must be accompanied by the swing-out of the hybrid domain for it to induce activation.

## DISCUSSION

By characterizing the recombinant αIIbβ3 integrin expressed in CHO cells, we established that αIIbβ3 constrained in its bent conformation represents a low affinity form, whereas αIIbβ3 constrained in its extended conformation represents a high affinity form. This constitutive activation depends on the swing-out of the hybrid domain because the prevention of this swing-out completely inhibited ligand binding regardless of the bent/extended state.

Integrin domains make large interdomain interfaces between the α-head and the β-head, the α-tail and the β-tail, and the β-head and the β-tail. Among these interfaces, the β-head/β-tail interface is presumed to play a central role in keeping integrin in its bent conformation because this is the only interaction that directly connects the head with the tail region in the bent conformer but not in the extended conformer. This interface is maintained by multiple interdomain interactions. The βA and the hybrid domains in the β-head make contact with the C-terminal βT domain. The hybrid domain also makes con-

tact with the EGF-3 and EGF-4 domains. We attempted to stabilize this interface by introducing artificial disulfide bridges between these domains. As previously reported, stabilizing the βA/βT interface (V332C/S674C) completely blocked Fbg binding (9). Likewise, stabilizing the hybrid/EGF-3 (S367C/S551C) or hybrid/EGF-4 (G382C/T564C) interface completely abolished Fbg binding. Regardless of the positions of the disulfide bridges that were introduced, stabilizing these interfaces prevented integrin from adopting the extended conformation. However, the S367C/S551C and G382C/T564C mutations not only prevented integrin extension but also restricted the relative movements of the hybrid and β-tail domains. For this reason, it might be premature to conclude that integrin extension is essential for activation. However, the fact that ligating the α-head with the β-tail or limiting αIIb extension using intrachain disulfide bridges that do not directly restrict hybrid/β-tail movement also prevented activation (9, 26) suggests that the completely bent conformer observed in the crystal structure represents the low affinity form rather than the high affinity form. These results also indicate that the β-head/β-tail interface must be disrupted all the way up to the linker region for the integrin to be activated.

The fact that the ligand-mimetic non-activation-dependent mAb OP-G2 did not bind to cells expressing the V332C/S674C mutant suggests that this mutant does not support low affinity ligand binding. In addition, anti-LIBS mAb binding to this particular mutant indicates that V332C/S674C is unable to undergo structural rearrangement in the presence of the RGD peptide. Taken together, these results suggest that the V332C/S674C mutant is not capable of binding either macromolecular ligands or ligands as small as the RGD peptide. Because the V332C/S674C mutation ligates the α7 helix in βA with the CD loop in βT, the possible downward movement of the α7 helix required for ligand binding in the integrin A domains would be inhibited. Thus, the effect of the V332C/S674C mutation is a combination of both β-head/β-tail stabilization and the inhibition of α7 helix movement. In agreement with these findings, the S367C/S551C mutation, which does not restrict α7 helix movement, only partially blocked OP-G2 binding (data not shown).

The contribution of each interface interaction in maintaining integrin in the bent conformation has not been clarified. It has been reported that replacing the β2 CD loop sequence with the homologous β3 sequence or inserting a *N*-glycan-binding site in the CD loop in αMβ2 integrin induced robust ligand binding (27). However, the fact that the deletion of the CD loop of the βT domain failed to activate αIIbβ3 in our experiment strongly argues against the deadbolt theory, in which an endogenous βA/βT interface interaction plays a critical role in maintaining integrin in its low affinity state. In addition, the insertion of a bulky *N*-glycan at the interface only slightly activated αIIbβ3 in the presence of $Ca^{2+}/Mg^{2+}$. These results suggest that hybrid/EGF-3, hybrid/EGF-4, and hybrid/βT interface interactions, rather than the βA/βT interface alone, play important roles in maintaining integrin in a low affinity state. In agreement with these conclusions, a computer-assisted approach has identified key interactions in the hybrid/β-tail interface in β3 integrin (28). Although the disruption of the hybrid/βT or the hybrid/EGF-3 interaction alone only produced weak activation, disrupting multiple interactions at the same time induced significant activation. Thus, the hybrid/β-tail interface seems to be maintained by a group of several key interactions that individually are not sufficiently strong to do so. The apparently distinct role of the βA/βT interface interaction in regulating activation in β2 and β3 integrins suggests that the contributions of each interdomain interaction to maintaining integrin in a low affinity state may differ among different integrin subfamilies.

A high resolution electron microscopic analysis of recombinant αVβ3 extracellular domains revealed that ligand-bound αVβ3 preferentially adopts an extended, rather than a bent, conformation (9). Based on these observations, it has been tentatively concluded that the extended conformer represents a high affinity form. The current study provides direct evidence that the highly extended conformer indeed has a higher ligand affinity than the completely bent conformer. Among the three mutants that showed constitutive Fbg binding in this study, β3S674N/K676T showed the lowest, αIIbQ595N/R597T showed the highest, and αIIbD589N/H591T showed an intermediate binding affinity. These results suggest that the degree of extension may be correlated with the extent of activation. These results also indicate that integrins are capable of assuming a wide range of affinity states depending on the degree of extension. Recently, it has been shown that integrin extension may not necessarily be accompanied by activation based on discrepancies between the expression of an extension-reporting epitope for KIM127 and an activation-reporting epitope for mAb24 on αLβ2 under flow conditions (29). It is possible that αA domain-containing integrin may require an additional step to achieve activation, unlike integrins without αA domains. It would be interesting to examine whether the introduction of a neoglycan that induces αL extension activates αLβ2.

Our results apparently contradict a report that αVβ3 is capable of binding fibronectin while in a bent conformation (14). However, it is not possible to tell to what degree integrin must extend to enable substantial ligand binding based on our experiments. The fact that αIIbβ3 can exist in a wide range of affinity states depending on the degree of the extension implies that as long as it is not completely bent, ligand binding could be observed to a varying extent. In other words, relaxation of the β-head/β-tail interface interaction, but not complete extension, may be sufficient for ligand binding to occur, especially in the presence of $Mn^{2+}$. As shown in Fig. 3*B*, $Mn^{2+}$ seems to lessen the requirement for integrin extension for Fbg binding. $Mn^{2+}$ activation alone has consistently been reported not to be accompanied by integrin extension (30). A recent report by Blue *et al.* (26) has provided a plausible explanation for the discrepancies in ligand binding observed under different cation conditions. Limiting αIIb extension using intrachain disulfides did not block Fbg binding in the presence of $Mn^{2+}$, although binding was blocked in the presence of $Ca^{2+}/Mg^{2+}$. In contrast, limiting β-head/β-tail movement using S367C/S551C, G382C/T564C, and V332C/S674C double mutations blocked Fbg binding significantly in the presence of $Mn^{2+}$ as well as in the presence of $Ca^{2+}/Mg^{2+}$ (data not shown). Taken together, these results may imply that it is not integrin extension *per se*, but

the relative β-head/β-tail movement (*e.g.* the swing-out of the hybrid domain), that is essential for activation in the presence of $Mn^{2+}$. These results may explain why ligand binding was observed for the bent conformer in some studies in which $Mn^{2+}$ was utilized to induce ligand binding (13, 14). Further study is required to determine the differences in the structural requirements for activation under different cation conditions.

Springer and co-workers (10, 23) have shown that ligand binding induces swing-out of the hybrid domain and that this change induces strong activation by itself, regardless of the bent/extend conformation. Our results show that the swing-out of the hybrid domain is essential for activation and that extension-induced activation absolutely depends on this change. These results indicate that the affinity state of the extended conformer is controlled by the swing-out of the hybrid domain and that to down-regulate activation, integrin does not necessarily need to go back to its original bent conformation but that this can rather be accomplished by the swing-in of the hybrid domain. Interestingly, constraining the integrin head in a closed state did not prevent OP-G2 binding at all (Fig. 6*B*). Unlike PAC-1, which binds αIIbβ3 in an activation-dependent fashion, OP-G2 is less dependent on integrin activation (18). This difference indicates that the swing-out of the hybrid domain is required only for high affinity ligand binding but not for low affinity ligand binding. However, we are not sure at this point whether the swing-out of the hybrid domain alone is sufficient for high affinity ligand binding, as reported by Springer and co-workers (23). Our experiments using recombinant αIIbβ3 expressed on the CHO cell surface have shown that the swing-out of the hybrid domain only induced moderate activation. To induce full activation, integrin extension was required.[5] It is possible that the proximity of the integrin head domains to the plasma membrane in the bent conformation may limit the access of macromolecular ligands. Experiments utilizing cell-free binding studies should help to clarify these discrepancies. Interestingly, anti-LIBS mAb binding was still observed in the closed head mutant (D319C/V359C) in the presence of RGD peptide. Because ligand binding induces the outward swing of the hybrid domain and this movement would probably disrupt the β-head/β-tail interface, it is reasonable to assume that this swing-out triggers the structural transition from a bent to an extended conformation in outside-in signaling. However, our result suggests the possibility that a structural change in addition to the swing-out may trigger the conformational change upon ligand binding. A recent report also suggests that integrin affinity may be regulated independently from the swing-out of the hybrid domain based on the expression of anti-LIBS epitope located in the hybrid domain (31). Because we do not know the specific conformation to which each of the anti-LIBS mAbs binds, further analysis is needed to address this issue.

Then, what triggers the structural transition from the bent to the extended conformation during inside-out signaling? Numerous studies have suggested the importance of integrin cytoplasmic tails in regulating integrin activation. It has been shown that integrin cytoplasmic tails undergo structural rearrangement upon ligand binding (32). It was subsequently shown that the two cytoplasmic tails separate from each other upon ligand binding (3). On the other hand, the deletion of the entire α or β cytoplasmic tail at the membrane-proximal sites induced significant activation (33). NMR studies on recombinant αIIbβ3 cytoplasmic tails have shown that talin binding to the β3 cytoplasmic tail disrupts the endogenous interaction between the α and β cytoplasmic tails (2). Because talin binding to the β3 cytoplasmic tail activates αIIbβ3, it was concluded that the separation of the two cytoplasmic tails somehow induces structural rearrangement of the integrin extracellular domains (1). We have previously shown that stabilizing the α-tail/β-tail interface with artificial disulfide bridges completely abolished the activation induced by cytoplasmic tail deletion (22). Based on these observations, we hypothesized that the separation of the two extracellular tails following the cytoplasmic tail dissociation induces structural rearrangement from the bent to the extended conformation. Indeed, the separation of the α-tail/β-tail interface induced robust activation.[6] The α-tail/β-tail interface and the β-head/β-tail interface are located next to each other, flanking the β-tail. Because the β-head/β-tail interface, and not the α-tail/β-tail interface, maintains integrin in its bent conformation, it is reasonable to assume that the separation of one interface destabilizes the other. Further elucidation of the role of these interface interactions in integrin affinity regulation will facilitate understanding of integrin-mediated bidirectional signaling.

*Acknowledgments—We thank Dr. Joseph C. Loftus for providing the αIIb, αV, and β3 cDNAs and Drs. Mark H. Ginsberg, Jari Ylänne, Ismo Virtanen, and Yoshiaki Tomiyama for providing the anti-αIIbβ3 mAbs.*

## REFERENCES

1. Calderwood, D. A., Zent, R., Grant, R., Rees, D. J., Hynes, R. O., and Ginsberg, M. H. (1999) *J. Biol. Chem.* **274,** 28071–28074
2. Vinogradova, O., Velyvis, A., Velyviene, A., Hu, B., Haas, T., Plow, E., and Qin, J. (2002) *Cell* **110,** 587–597
3. Kim, M., Carman, C. V., and Springer, T. A. (2003) *Science* **301,** 1720–1725
4. Frelinger, A. L., 3rd, Cohen, I., Plow, E. F., Smith, M. A., Roberts, J., Lam, S. C., and Ginsberg, M. H. (1990) *J. Biol. Chem.* **265,** 6346–6352
5. Du, X. P., Plow, E. F., Frelinger, A. L., 3rd, O'Toole, T. E., Loftus, J. C., and Ginsberg, M. H. (1991) *Cell* **65,** 409–416
6. Carrell, N. A., Fitzgerald, L. A., Steiner, B., Erickson, H. P., and Phillips, D. R. (1985) *J. Biol. Chem.* **260,** 1743–1749
7. Weisel, J. W., Nagaswami, C., Vilaire, G., and Bennett, J. S. (1992) *J. Biol. Chem.* **267,** 16637–16643
8. Xiong, J. P., Stehle, T., Diefenbach, B., Zhang, R., Dunker, R., Scott, D. L., Joachimiak, A., Goodman, S. L., and Arnaout, M. A. (2001) *Science* **294,** 339–345
9. Takagi, J., Petre, B. M., Walz, T., and Springer, T. A. (2002) *Cell* **110,** 599–611
10. Takagi, J., Strokovich, K., Springer, T. A., and Walz, T. (2003) *EMBO J.* **22,** 4607–4615
11. Xiao, T., Takagi, J., Coller, B. S., Wang, J. H., and Springer, T. A. (2004) *Nature* **432,** 59–67
12. Adair, B. D., and Yeager, M. (2002) *Proc. Natl. Acad. Sci. U.S.A.* **99,**

[5] T. Kamata, M. Handa, S. Ito, Y. Sato, T. Ohtani, Y. Kawai, Y. Ikeda, and S. Aiso, unpublished data.

[6] T. Kamata, M. Handa, Y. Kawai, Y. Ikeda, and S. Aiso, manuscript in preparation.

14059–14064
13. Xiong, J. P., Stehle, T., Zhang, R., Joachimiak, A., Frech, M., Goodman, S. L., and Arnaout, M. A. (2002) *Science* **296,** 151–155
14. Adair, B. D., Xiong, J. P., Maddock, C., Goodman, S. L., Arnaout, M. A., and Yeager, M. (2005) *J. Cell Biol.* **168,** 1109–1118
15. Adair, B. D., and Yeager, M. (2007) *Methods Enzymol.* **426,** 337–373
16. Ylänne, J., Hormia, M., Järvinen, M., Vartio, T., and Virtanen, I. (1988) *Blood* **72,** 1478–1486
17. Frelinger, A. L., 3rd, Du, X. P., Plow, E. F., and Ginsberg, M. H. (1991) *J. Biol. Chem.* **266,** 17106–17111
18. Tomiyama, Y., Tsubakio, T., Piotrowicz, R. S., Kurata, Y., Loftus, J. C., and Kunicki, T. J. (1992) *Blood* **79,** 2303–2312
19. Tokuhira, M., Handa, M., Kamata, T., Oda, A., Katayama, M., Tomiyama, Y., Murata, M., Kawai, Y., Watanabe, K., and Ikeda, Y. (1996) *Thromb. Haemost.* **76,** 1038–1046
20. Kamata, T., Irie, A., Tokuhira, M., and Takada, Y. (1996) *J. Biol. Chem.* **271,** 18610–18615
21. Zhu, J., Luo, B. H., Xiao, T., Zhang, C., Nishida, N., and Springer, T. A. (2008) *Mol. Cell* **32,** 849–861
22. Kamata, T., Handa, M., Sato, Y., Ikeda, Y., and Aiso, S. (2005) *J. Biol. Chem.* **280,** 24775–24783
23. Luo, B. H., Springer, T. A., and Takagi, J. (2003) *Proc. Natl. Acad. Sci. U.S.A.* **100,** 2403–2408
24. Kamata, T., Tieu, K. K., Irie, A., Springer, T. A., and Takada, Y. (2001) *J. Biol. Chem.* **276,** 44275–44283
25. Tomiyama, Y., Brojer, E., Ruggeri, Z. M., Shattil, S. J., Smiltneck, J., Gorski, J., Kumar, A., Kieber-Emmons, T., and Kunicki, T. J. (1992) *J. Biol. Chem.* **267,** 18085–18092
26. Blue, R., Li, J., Steinberger, J., Murcia, M., Filizola, M., and Coller, B. S. (2010) *J. Biol. Chem.* **285,** 17604–17613
27. Gupta, V., Gylling, A., Alonso, J. L., Sugimori, T., Ianakiev, P., Xiong, J. P., and Arnaout, M. A. (2007) *Blood* **109,** 3513–3520
28. Matsumoto, A., Kamata, T., Takagi, J., Iwasaki, K., and Yura, K. (2008) *Biophys. J.* **95,** 2895–2908
29. Kuwano, Y., Spelten, O., Zhang, H., Ley, K., and Zarbock, A. (2010) *Blood* **116,** 617–624
30. Ye, F., Liu, J., Winkler, H., and Taylor, K. A. (2008) *J. Mol. Biol.* **378,** 976–986
31. Chigaev, A., Waller, A., Amit, O., Halip, L., Bologa, C. G., and Sklar, L. A. (2009) *J. Biol. Chem.* **284,** 14337–14346
32. Leisner, T. M., Wencel-Drake, J. D., Wang, W., and Lam, S. C. (1999) *J. Biol. Chem.* **274,** 12945–12949
33. Hughes, P. E., O'Toole, T. E., Ylänne, J., Shattil, S. J., and Ginsberg, M. H. (1995) *J. Biol. Chem.* **270,** 12411–12417

J Biorheol (2009) 23:35–40
DOI 10.1007/s12573-009-0007-y

ORIGINAL ARTICLE

# Deformability and adhesive force of artificial platelets measured by atomic force microscopy

**Toru Wada · Yosuke Okamura · Shinji Takeoka · Ryo Sudo · Yasuo Ikeda · Kazuo Tanishita**

Received: 10 January 2009 / Accepted: 30 April 2009 / Published online: 2 July 2009


**Abstract** Platelet glycoprotein GPIaIIa is an adhesive protein that recognizes collagen. We have investigated polymerized albumin particles conjugated with recombinant GPIaIIa (rGPIaIIa-poly Alb) for their platelet-like function. To evaluate the feasibility of these particles to achieve the hemostatic process, we measured the deformability (Young's modulus and spring constant) and the adhesive force of the particles using atomic force microscopy, which can measure the mechanical properties of individual cells. Our results showed that the Young's modulus of these particles was 2.3-fold larger than that of natural platelets and 12-fold larger than that of human red blood cells. The Young's modulus of the particles may have been determined by the properties of the polymerized albumin particle, although the glycoprotein of the platelet surface also contributed to the higher modulus. Our results also showed that the adhesive force of the rGPIaIIa-poly Alb with the collagen ligand was 52% of that of natural platelets. These two mechanical properties (deformability and adhesive force) of cells or particles, such as rGPIaIIa-poly Alb, are important specifications for the optimum design of platelet substitutes.

**Keywords** Adhesive force · Atomic force microscopy · Deformability · Glycoprotein GPIaIIa · Platelet substitutes · Thrombocytopenia · Young's modulus

T. Wada · K. Tanishita (✉)
Department of System Design Engineering,
Keio University, 3-14-1 Hiyoshi, Kohoku-ku,
Yokohama 223-8522, Japan
e-mail: tanishita@sd.keio.ac.jp

Y. Okamura · S. Takeoka
Department of Life Science and Medical Bioscience,
Waseda University, 3-4-1 Ohkubo,
Shinjuku-ku, Tokyo 169-8555, Japan

R. Sudo
Department of Biological Engineering,
Massachusetts Institute of Technology,
Cambridge, MA 02139-4307, USA

Y. Ikeda
School of Medicine, Keio University,
35 Shinanomachi, Shinjuku-ku, Tokyo 160-8582, Japan

## Introduction

The total amount of platelets transfused annually worldwide has grown rapidly in recent years [1] primarily because platelet transfusion is the most effective therapy for bleeding associated with chemotherapy-induced thrombocytopenia or thrombocytopenia that develops following surgery. However, it is difficult to meet such a large demand for platelets due to their storage being limited to short-term periods and the risks involved in platelet transfusion, such as viral infections [2–4].

These difficulties can be overcome and the increased demand can be met by the use of platelet substitutes. The first of these was developed by Coller in 1980 [1] in the form of fibrinogen-coated beads that interacted with natural platelets, and numerous prototypes of platelet substitutes have been developed since [5, 6]. For example, Murata et al. [7] developed rGPIbα-liposomes, which are produced by incorporating a recombinant glycoprotein (GP)Ibα (an adhesive receptor on a platelet) to phospholipid bilayers of liposomes. Specific agglutination of rGPIbα-liposome to platelets occurs in the presence of von Willebrand factor (VWF) and ristocetin [8]. More recently, Takeoka et al. [9] developed polymerized albumin particles conjugated with recombinant glycoprotein Ibα (rGPIbα-poly Alb) and demonstrated (in in vitro experiments) the shear-

dependent adhesive property. In this type of platelet substitute, rGPIa/IIa-poly Alb, the glycoprotein GPIa/IIa is a receptor to the ligand of collagen and adheres to the collagen surface. The polymerized albumin particles represent a promising carrier for functional proteins because of their high blood compatibility and high biodegradability as well as the fact that they have been the subject of long-term study in clinical applications [10].

The major functions of platelets are adhesion and agglutination to the vascular injury region; consequently, the adhesive force is a major key to achieving such platelet functions. Therefore, any study that evaluates the feasibility of a platelet substitute to achieve the thrombogenic process must also determine the adhesive force of that platelet substitute. Atomic force microscopy (AFM) is the ideal method for measuring this adhesive force [11] because it can trace the surface topography of an individual living cell in a physiological medium and measure the adhesive force and elasticity of this cell by mapping the interactive forces.

A number of studies have demonstrated the effectiveness of using the AFM to measure the adhesive forces in cells. Lee et al. [12] directly measured the adhesive force of receptor-ligand and antibody–antigen associations in the immune system at a sensitivity of $10^{-14}$ N using AFM. Florin et al. [13] measured the adhesive force of the biotin–avidin association. (Biotin is a vitamin B complex and becomes inactivated by coupling with avidin specifically.) In their study, the $Si_3N_4$ tip of the AFM was first coated with bovine serum albumin (BSA), which adheres to biotin, and then the adhesive force was measured (160 ± 20 pN). Lee et al. [12] measured the adhesive force of streptavidin–biotin interactions under physiological conditions and identified the adhesive force to be due to individual streptavidin–biotin interactions. Holland et al. [14] measured the adhesive force of platelets adsorbed into a collagen substrate by using peptide-coated tips.

Another important mechanical property of platelets is deformability because it affects the lateral motion and aggregation process of platelets in the blood flow [15]. The deformability of platelets significantly affects the rolling and tethering of the platelets on the vascular surface. Therefore, a comprehensive evaluation of the feasibility of platelet substitutes involves the determination of both their adhesive force and deformability. Two measurable indicators of deformability are the spring constant and Young's modulus (elastic modulus). The deformability of red blood cells has been used as an important clinical diagnostic parameter; for example, Minamitani et al. [16] found that the Young's modulus of red blood cells from diabetic patients was higher than that from healthy patients.

In the study reported here, we have used AFM to measure the adhesive force, spring constant, and Young's modulus of platelet substitutes developed by Takeoka et al. [9], which are polymerized albumin particles conjugated with recombinant glycoprotein (rGPIa/IIa-poly Alb). For comparison, the same properties were measured for human red blood cells, poly Alb alone, and natural platelets, and for the respective aggregates of rGPIa/IIa-poly Alb, poly Alb, and natural platelets (activated by ADP for aggregation).

## Materials and methods

### Preparation of artificial platelets

In the platelet substitutes used here (rGPIa/IIa-poly Alb), the glycoprotein GPIa/IIa (Toray Industries, Toyko, Japan) is a receptor to the ligand of collagen and adheres to the collagen surface. The preparation of the polymerized albumin particles (poly Alb) has been described previously [9]. Here, the poly Alb was prepared in aqueous solutions to retain the hydrophilicity on the surface to ensure a high dispersing ability and a high capability for conjugation with water-soluble functional proteins. The size of rGPIa/IIa-poly Alb ranged from 1 to 2 μm. To monitor and therefore ensure the presence of rGPIa/IIa-poly Alb on the surface of the dish used in experiments, the particles were labeled with a fluorescein isothiocyanate (FITC) dye.

### Preparation of red blood cells and natural platelets

Red blood cells (RBCs) were prepared as follows. Fresh human blood (9 ml) from healthy volunteers was added to a 0.29 *M* sodium citrate solution and then centrifuged at 156 *g* for 10 min. The resulting red cell pellets were rinsed with phosphate buffered saline (PBS) four times and then suspended in PBS to measure the deformability by AFM.

Natural platelets, as a platelet-rich plasma (PRP), were prepared as follows. Fresh human blood (9 ml) from healthy volunteers was added to a 0.013 *M* sodium citrate solution and centrifuged at 22,500 *g* for 15 s to separate PRP from the supernatant. The supernatant with free HEPES–Tyrode buffer was then centrifuged four times at 22,500 *g* for 15 s each time. The resulting supernatant with HEPES–Tyrode buffer was then mixed with 1.25 m*M* $CaCl_2$ and 6.25 mg/ml BSA and centrifuged at 352 *g* for 1 min. The final supernatant was PRP, which was then labeled with fluorescent probe carboxyfluorescein succinimidylester (CFSE) for visualization. Platelet aggregates were formed by adding ADP to the PRP, which activated the platelets.

Red cell ghosts were prepared from blood drawn from healthy volunteers into syringes containing a 0.29 *M* sodium citrate solution and then processed using the

hypotonic lysis method by Dodge et al. [17]. The resulting hematocrit was adjusted to 40% with PBS.

### Immobilization of cells and particle samples

For immobilization, poly Alb, rGPIa/IIa-poly Alb, and PRP were individually mixed with PBS, placed on the surface of a sampling dish for 1 h at 4°C, and then rinsed four times with PBS. The FITC-labeled particles of poly Alb and rGPIaIIa-poly Alb were immobilized on the surface of the dish and confirmed by fluorescent microscopy.

### Atomic force microscopy

The AFM system used to measure the adhesive force, spring constant, and Young's modulus of the immobilized cells and particles was a scanning probe microscope (NVB100; Olympus, Tokyo, Japan). The AFM probe was a cantilever (length 3 μm, curvature radius 15–20 nm) with a $Si_3N_4$ tip, and it had a spring constant of 0.09 N/m.

### Measurement of deformability

The spring constant and Young's modulus were measured for natural platelets, rGPIa/IIa-poly Alb, poly Alb, RBC ghost, and RBCs. The spring constant was determined based on Hook's law, namely, by determining the gradient of the measured force curve. Figure 1 illustrates the contact process between the AFM cantilever and the sample surface. After the tip on the cantilever contacts with the sample surface, the cantilever starts to slightly deform upward, generating a compressive force on the sample and thus distorting the sample. The compressive force of the cantilever was measured as a function of this distortion of the sample. A plot of the compressive force versus distortion is referred to as the force curve (Fig. 1b). Assuming that the cell behaves as a spring, the spring constant $K$ of the cell was calculated as

$$K = ky/(x - y) \tag{1}$$

where $k$ is the spring constant of the cantilever, $x$ is the displacement of the cantilever, and $y$ is the deformation of the cantilever.

The Young's modulus of the cells or particles was determined based on the Hertz contact theory [18], which gives the mechanical relation between a sphere and a plane surface. Based on this Hertz contact theory, the tip surface was approximated as a sphere of curvature radius $R$; therefore, Young's modulus $E$ of the cell was

$$E = \frac{3}{4}\frac{(1 - v^2) \times k}{R^{0.5}}\frac{y}{(x - y)^{1.5}} \tag{2}$$

where $v$ is the Poisson ratio of the cell or particle and was assumed to be 0.5. $R$ is the radius of tip—20 nm in this case. Thus, $E$ was determined by this expression based on the force curve.

### Modification of the AFM probe

To measure the adhesive force of the cells and particles, the $Si_3N_4$ tip of the AFM must be coated with collagen type I (which is in subendothelial cells) in order to bind the GPIaIIa onto the surface of platelets. To coat the tip, the cantilever was incubated at 4°C for 24 h in a solution of 0.3 mg/ml collagen type I (pH 3) and then dried. The adhesive force was also measured using an uncoated probe to determine the adhesive force between $Si_3N_4$ and the sample cells or particles.

### Measurement of adhesive force

The adhesive force of natural platelets, poly Alb, and rGPIaIIa-poly Alb was measured by drawing the cantilever away from the sample (Fig. 2a). Figure 2b illustrates the force curve used to determine the adhesive force. The adhesive force is the force generated by glycoprotein molecules (rGPIa/IIa) on the surface of poly Alb, which are activated by the collagen on the probe tip. The cantilever was deformed downward due to the adhesive force between the probe tip and the sample. The adhesive force $F$ was determined by the deformation and spring constant $k$ (= 0.09 N/m) of the cantilever as follows,

$$F = k\delta \tag{3}$$

## Results and discussion

Figure 3 shows the measured spring constant and Young's modulus of natural platelets, rGPIa/IIa-poly Alb, poly Alb, RBC ghosts, and RBCs. The Young's modulus of RBCs was the lowest and is consistent with that of RBCs measured by Minamitani et al. [16]. The lower Young's modulus of RBCs has physiological implications; RBCs have a highly flexible structure that allow them to penetrate into narrow capillary vessels. Because the deformability of RBCs significantly affects the non-Newtonian nature of blood flow, many previous studies have focused on the influence of the deformability of RBCs on the lateral movement of cells [15]. However, a direct measurement of such deformability of RBCs is difficult due to the complicated shape of these cells. Many of the common measurement modalities used in earlier studies, such as micropipette aspiration, do not explicitly determine the elasticity of RBCs because of the complicated deformation

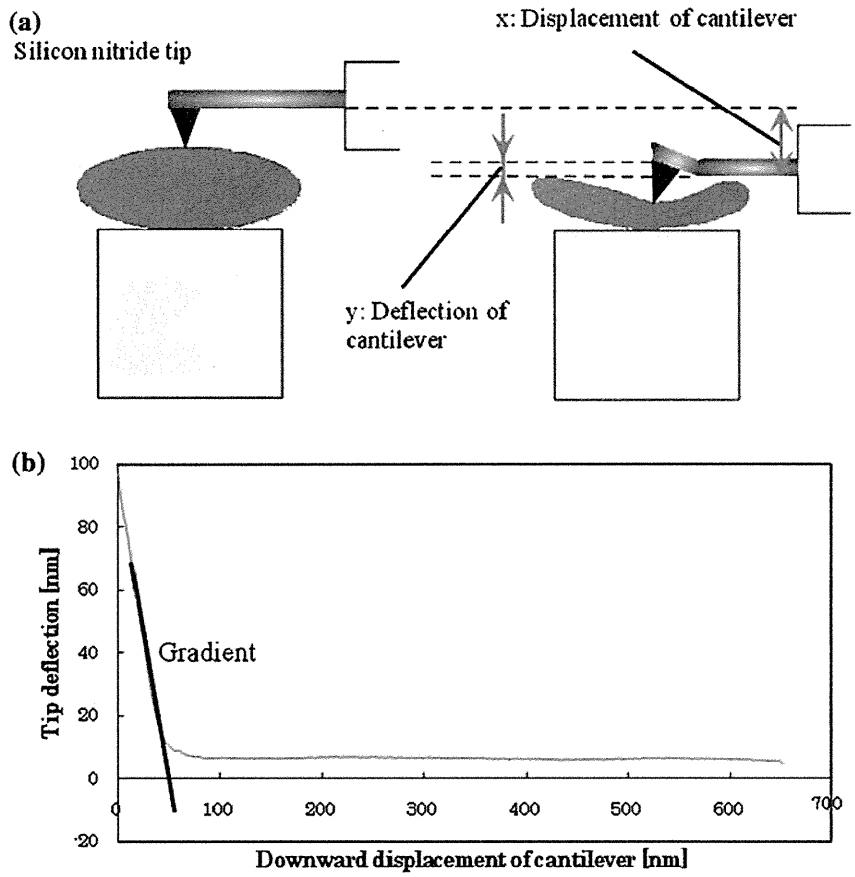


**Fig. 1** **a** Schematic of cantilever displacement and deformation to measure the Young's modulus and spring constant of an individual cell or particle using an atomic force microscopy system. **b** The force curve

process [19]. In contrast, AFM provides a simple technique by which to determine the localized elasticity of an RBC membrane. The Young's modulus of the RBC ghosts was larger than that of the RBCs, possibly due to the processing of the RBC membrane during the preparation of the RBC ghosts. In comparison, the Young's modulus of the natural platelets was larger than that of the RBC ghosts, probably because a natural platelet is filled with intracellular structures, whereas RBCs and RBC ghosts consist of highly flexible membranes. The Young's modulus of poly Alb was larger than that of the natural platelets because poly Alb consists of packed polymerized albumin molecules, and the Young's modulus of rGPIa/IIa-poly Alb was slightly larger than that of poly Alb.

The Young's modulus was determined based on the force curve, which was not completely linear. In general, mechanical properties of RBCs are non-linear due to the viscoelastic properties of these cells, and Young's modulus of a cell or particle depends on deformation. In this study, therefore, the gradient of the force curve was determined from a linear portion of the force curve, namely, a small deformation range, which resulted in a Young's modulus of the natural platelets of 28 ± 9.8 kPa, compared with 5–50 kPa reported by Lee et al. [20].

Figure 4 shows the adhesive force measured using AFM. The adhesive force determined from the force curve reflects the interaction between the cell or particle and AFM tip surface. Thus, the tip surface significantly affects the interaction and, therefore, the adhesive force depends on the condition of the collagen coating. To confirm the effectiveness of collagen coating, we measured the adhesive force using a tip that was not coated with collagen. For all three samples (platelet, poly Alb with GPIa/IIa, and poly Alb without GPIa/IIa), the adhesive force measured with an uncoated tip was almost constant, indicating that the uncoated tip itself generated a slight interactive force of approximately 20 pN. To evaluate the actual adhesive force of the cell or particle, we subtracted this slight interactive force from the force measured with the coated tip for all three samples.

Figure 4 shows that the measured adhesive force of rGPIa/IIa-poly Alb was fourfold larger than that of poly Alb alone (without the glycoprotein rGPIa/IIa) and about half that of the natural platelets. Holland et al. [14] measured the adhesive force of natural platelets using AFM with a peptide-coated probe. The integrin receptor GPIIb/IIIa, which is a glycoprotein also found in the platelet, generated an interactive force with the probe. Holland et al.

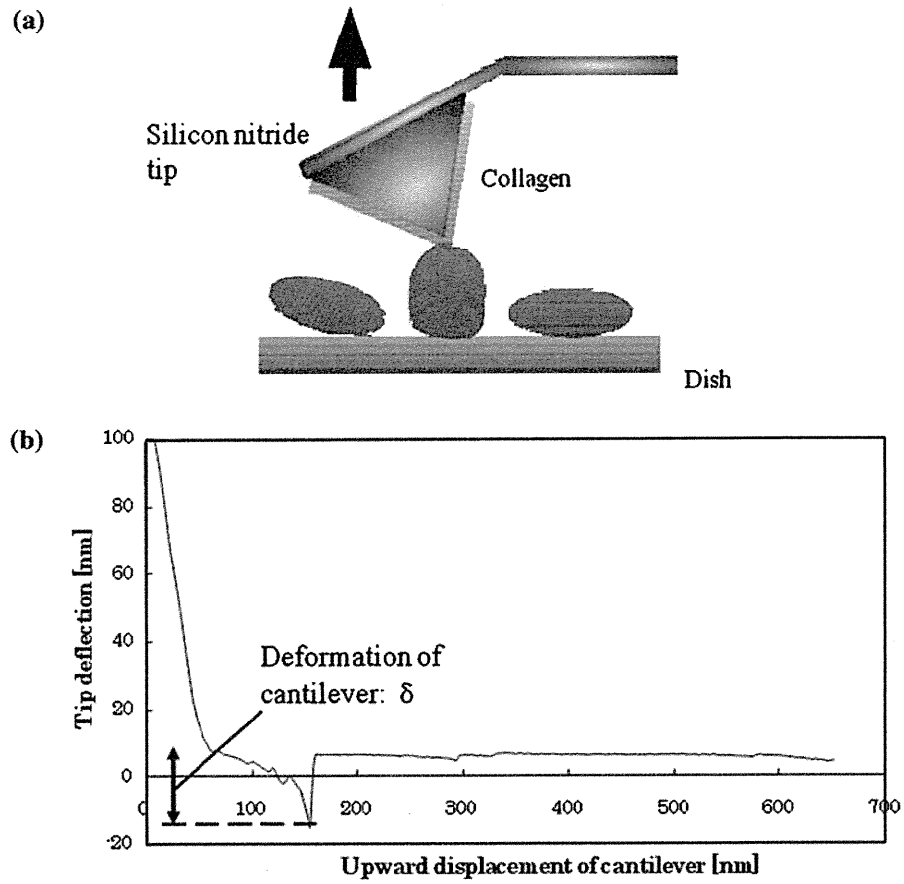


**Fig. 2** **a** Schematic of cantilever displacement and deformation to measure the adhesive force between the receptor (glycoprotein rGPIa/IIa) and ligand (collagen) using an AFM system. **b** The force curve

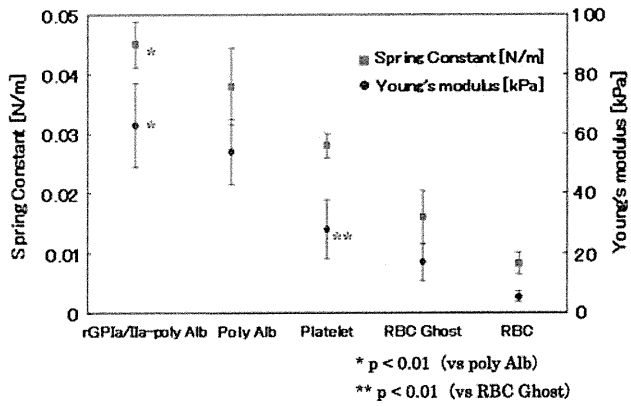


**Fig. 3** Young's modulus and spring constant of an individual polymerized albumin particle (*poly Alb*) conjugated with the recombinant glycoprotein GPIaIIa (*GPIa/IIa-poly Alb*), poly Alb, natural platelet, red blood cell (*RBC*) ghost, and RBC, as measured using AFM. $*p < 0.01$ (vs. poly Alb), $**p < 0.01$ (vs. RBC ghost)

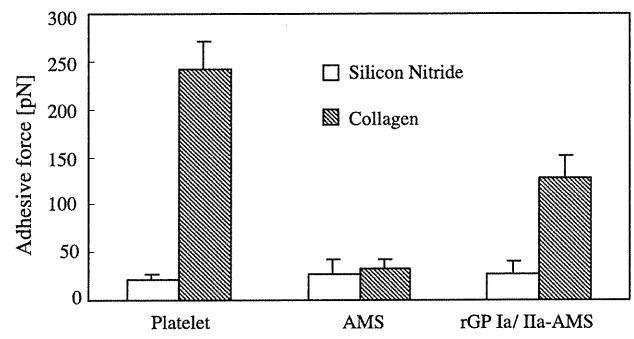


**Fig. 4** Adhesive force of an individual natural platelet, poly Alb, and rGPIa/IIa-poly Alb, as measured by AFM

[14] also showed that a tip coated with an oligopeptide, GGGRGD, yielded an adhesive force of 660 pN and that a probe coated with GDGGAR, yet another oligopeptide, generated an adhesive force of 320 pN. In our study, the adhesive force of natural platelets was 242 ± 29 pN, which is close to that of the oligopeptide GDGGAR reported by Holland et al. [14], although the adhesive mechanism with peptides is different from that with collagen. In our study, the tip was coated with a collagen that is the ligand for a receptor of GPIa/IIa in the platelet. Because a platelet generates an adhesive force caused by the multi-site interaction with other receptors, such as GPIb

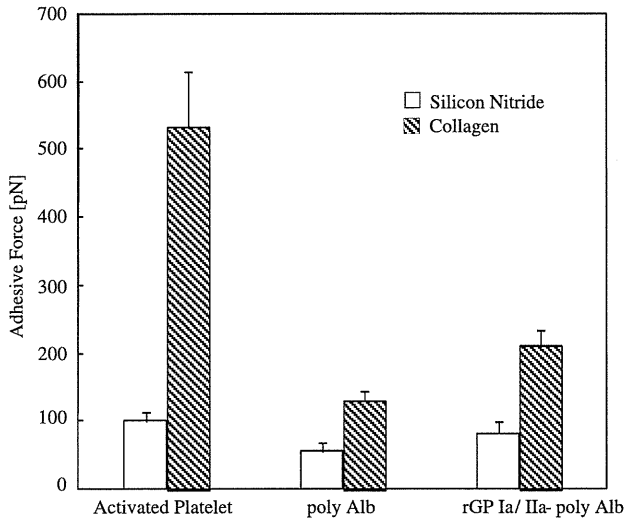


**Fig. 5** Adhesive force of aggregates of natural platelets, poly Alb, and rGPIa/IIa-poly Alb, as measured by AFM

and GPIIb/IIIa, the adhesive force that we measured is only a part of the adhesive ability of natural platelets.

Figure 5 shows the measured adhesive force for the aggregates of cells and particles. All of the aggregates had an adhesive force larger than that of their respective single cell or particle because an adhesive force is generated between the AFM tip and aggregates. The adhesive force of the platelet aggregates was twice as large as that of a single platelet, and that of rGPIa/IIa-poly Alb was 64% larger than that of a single particle.

This study revealed that force mapping using AFM can quantify the adhesive force and deformability of an individual cell or particle. For artificial platelets, both of these properties are affected by the nature of the particle itself (e.g., albumin microspheres) and by the distribution of the receptor molecules (e.g., recombinant glycoprotein GPIaIIa) on the surface of the particle. These two mechanical properties are important specifications to be taken into account for the optimum design of artificial platelets, and their evaluation can be used to determine the feasibility of using artificial platelets.

**Acknowledgment** This work was supported by Health Science Research Grants (Artificial Platelets) from the Research on Advanced Medical Technology, Ministry of Health, Labour and Welfare, Japan.

## References

1. Coller BS. Interaction of normal thrombasthetic and Bernard–Soulier platelets with immobilized fibrinogen: defective platelet–fibrinogen interaction in thrombasthenia. Blood. 1980;55:169–78.
2. George JN. Changes in platelet membrane glycoprotein during blood bank storage. Blood Cells. 1992;18:501–11.
3. Eaton LA, Read MS, Brinkhous KM. Glycoprotein Ib assays. Activity levels in Bernard–Soulier syndrome and in stored blood bank platelets. Arch Pathol Lab Med. 1991;115:488–93.
4. Kickler TS. Improving the quality of stored platelets. Transfusion. 1991;31:1–3.
5. Agam G, Livne A. Passive participation of fixed platelets in aggregation facilitated by covalently bound fibrinogen. Blood. 1983;61(1):186–91.
6. Agam G, Livne A. Erythrocytes with covalently bound fibrinogen as a cellular replacement for the treatment of thrombocytopenia. Eur J Clin Invest. 1992;22(2):105–12.
7. Murata M, Ware J, Ruggeri ZM. Site-directed mutagenesis of a soluble fragment of platelet glycoprotein Ibα demonstrating negatively charged residues involved in von Willebrand factor binding. J Biol Chem. 1991;266:15474–80.
8. Kitaguchi T, Murata M, Iijima K, Kamide K, Imagawa T, Ikeda Y. Characterization of liposomes carrying von Willebrand factor-binding domain of platelet glycoprotein Ibalpha: a potential substitute for platelet transfusion. Biochem Biophys Res Commun. 1999;261(3):784–9.
9. Takeoka S, Teramura Y, Ohkawa H, Ikeda Y, Tsuchida E. Conjugation of von Willebrand factor-binding domain of platelet glycoprotein Ibα to size-controlled albumin microspheres. Biomacromolecules. 2000;1(2):290–5.
10. Gupta PK, Hung CT. Albumin microsphere I: physicochemical characteristics. J Microencapsul. 1989;6:262–427.
11. Jena BP, Hörber JKH. Atomic force microscopy in cell biology. San Diego: Academic Press; 2002. p. 67.
12. Lee GU, Kidwell DA, Colton RJ. Sensing discrete streptavidin–biotin interactions with atomic force microscopy. Langmuir. 1994;10:354–7.
13. Florin EL, Moy VT, Gaub E. Adhesion forces between individual ligand-receptor pairs. Science. 1994;264:415–7.
14. Holland NB, Siedlecki CA, Marchant RE. Intermolecular force mapping of platelet surfaces on collagen substrata. J Biomed Mater Res. 1999;45:167–74.
15. Goldsmith HL, Marlow JC. Flow behavior of erythrocytes. J Colloid Interface Sci. 1979;71(2):383–407.
16. Minamitani H, Kawamura T, Tsukada T, Iijima A, Sekizuka E, Osho C. Measurement of elasticity of erythrocytes using atomic force microscope. Trans IEE Jpn. 2002;122:1664–71.
17. Dodge JT, Mitchell C, Hanahan DJ. The preparation and chemical characteristics of hemoglobin-free ghosts of human erythrocytes. Arch Biochem Biophys. 1962;100:119.
18. Hertz H. Über die Berühung fester elastischer Körper. J Reine Angew Math. 1882;92:156–71.
19. Evans EA, Skalak R. Mechanics and thermodynamics of biomembranes, CRC critical reviews in Bioengineering. vol. 3, issues 3 & 4. Boca Raton: CRC Press; 1979.
20. Lee IS, Marchant RE. Force measurements on platelet surfaces with high spatial resolution under physiological conditions. Colloids Surf B Biointerfaces. 2000;19:357–65.